Expression of Rab3D N135I Inhibits Regulated Secretion of ACTH in AtT-20 Cells

Giulia Baldini,* Giovanna Baldini,‡ Guangyi Wang,* Mattew Weber,* Marina Zweyer,‡ Renato Bareggi,‡ Joan W. Witkin,* and Alberto M. Martelli‡

*Department of Anatomy and Cell Biology, Columbia University, College of Physicians and Surgeons, New York, 10032; and ‡Dipartimento di Morfologia Umana Normale, University of Trieste, Trieste, Italy I-34138

Abstract. Rab proteins are small molecular weight GTPases that control vesicular traffic in eucaryotic cells. A subset of Rab proteins, the Rab3 proteins are thought to play an important role in regulated exocytosis of vesicles. In transfected AtT-20 cells expressing wild-type Rab3D, we find that a fraction of the protein is associated with dense core granules. In the same cells, expression of a mutated isoform of Rab3D, Rab3D N135I, inhibits positioning of dense core granules near the plasma membrane, blocks regulated secretion of mature ACTH, and impairs association of Rab3A to membranes. Expression of Rab3D N135I does not change the levels of ACTH precursor or the efficiency with which the precursor is processed into ACTH hormone and packaged into dense core granules. We also find that cells expressing mutated Rab3D differentiate to the same extent as untransfected AtT-20 cells. We conclude that expression of Rab3D N135I specifically impairs late membrane trafficking events necessary for ACTH hormone secretion.

RAB proteins are small monomeric GTPases proposed to function as key regulators of vesicular traffic (33, 38). Rab3 proteins, a family of highly homologous Rab isoforms, are abundant in cells with regulated secretory pathways (14). There are four Rab3 isoforms known: Rab3A, Rab3B, Rab3C, and Rab3D (1, 27, 43, 51). In neurons, Rab3A and Rab3C are associated with synaptic vesicles (12, 13). In adrenal medullary cells and rat islets, Rab3A is associated with hormone-containing secretory granules (7, 8, 34). Rab3B is abundant in epithelial cells (49). Rab3D is found associated with zymogen-containing granules in the acinar cells of the pancreas and in the chief cells of gastric glands (41, 44).

The exact role of Rab3 proteins in regulated exocytosis is unknown. Rab3A is involved in neurotransmission. Transgenic mice lacking Rab3A have depressed synaptic transmission after repetitive stimulation (5, 16, 17). Functional data indicate that Rab3A and Rab3C dissociate from synaptic vesicles during neurotransmitter release (13, 15). Rab3A dissociation is coupled to GTP hydrolysis, indicating that the GTP/GDP cycle of Rab3A is important for regulated exocytosis (39). In PC12 cells, adrenal chromaffin cells, and insulin-secreting cells, overexpression of Rab3A inhibits Ca^{2+}-dependent exocytosis of dense core granules (20, 22, 34). In PC12 cells, overexpression of Rab3B or mutated Rab3B N135I stimulates norepinephrine secretion (50). Rab3A and Rab3B may function as positive and negative regulators of epinephrine release, respectively. Members of the Rab3 family have also been shown to regulate exocytosis of zymogen-containing granules (21, 32), degranulation in mast cells (31), and exocytosis in pituitary cells (24). Rab3 isoforms may also regulate intracellular targeting of exocytotic vesicles to their release site (30).

AtT-20 cells are neuroendocrine cells that express proopiomelanocortin and process it into mature ACTH hormone (18, 25, 35). AtT-20 cells have constitutive secretory vesicles and dense core granules that release ACTH hormone in response to stimulation by secretagogues (19). Both constitutive and regulated secretory vesicles are accumulated at the tips of the processes (28). To investigate the role of Rab3D in exocytosis, we have transfected AtT-20 cells with a mutated isoform of Rab3D, Rab3D N135I. The analogous mutation in Sec4 (Sec4 N133I; 48) or Rab3A (Rab3A N135I; 4) makes these proteins unable to bind GTP. Sec4 N133I and Rab3A N135I behave as dominant-negative mutations and inhibit constitutive and regulated secretion, respectively (22, 48). We predicted that Rab3D N135I, when expressed in AtT-20 cells, would act as a dominant-negative mutant. We find that expression of Rab3D N135I induces changes in the distribution of dense core granules and impairs regulated secretion of ACTH.

Address all correspondence to Giulia Baldini, Department of Anatomy and Cell Biology, Columbia University, College of Physicians and Surgeons, New York, NY 10032. Tel.: (212) 305-6405. Fax: (212) 328-3890. E-mail: gb74@columbia.edu

Materials and Methods

Materials

Rabbit polyclonal antibodies against the amino-terminal region of Rab3D were previously described (2). The monoclonal antibodies CL 42.2 against Rab3A (29) and monoclonal antibodies against synaptobrevin II/vesicle-associated membrane protein (VAMP)[1]-2 were provided by R. Jahn (Yale University School of Medicine, New Haven, CT) (10, 46). Rabbit polyclonal antibody against Rab4 was provided by P. van der Sluijs (Utrecht University, Utrecht, the Netherlands) (45). The following reagents were purchased from commercial sources: monoclonal antibodies against synaptosomal-associated protein of 25 kD (SNAP-25) from Sternberger Monoclonals Inc. (Baltimore, MD); monoclonal antibodies against synaptotagmin from Stressgen Biotechnologies Corp. (Victoria, British Columbia, Canada); mouse monoclonal antibodies against ACTH 1-24 from Peninsula Laboratories Inc. (Belmont, CA); Cy3-conjugated donkey anti–mouse IgG and FITC-conjugated donkey anti–rabbit IgG from Jackson ImmunoResearch Laboratories Inc. (West Grove, PA), 10 nm colloidal gold-labeled protein A from Sigma Chemical Co. (St. Louis, MO).

Subcellular Fractionation, Sodium Carbonate Extraction, Gel Electrophoresis, and Immunoblotting

P2 fraction was prepared as described by Gumbiner et al. (18). Separation of proteins by SDS-PAGE, immunoblotting, densitometry, and protein determination were all performed as described (37).

Preparation of Rab3D N135I

A fragment of Rab3D cDNA containing the whole coding region was excised from pcDNA1 plasmid with BamH1 and BanI. Recessed 3′ termini were filled with Klenow fragment of *Escherichia coli* DNA polymerase I and subcloned into the SmaI site of pBluescript SK II vector (Stratagene, La Jolla, CA). Site-directed mutagenesis (Kunkel, 1985) was done with a kit (Muta-Gene Phagemid *in vitro* Mutagenesis Kit; Bio-Rad Laboratories, Hercules, CA), according to the manufacturer's instructions. Rab3D N135I, in which Asn-135 of Rab3D was changed to Ile-135, was generated using the mutagenic oligonucleotide primer 5′-CAG GTC ACA CTT AAT CCC CAC GAG GAT-3′. The mutation was confirmed by sequencing of the entire coding region. Rab3D and Rab3D N135I cDNAs were excised from pBluescript SK II vector with XhoI, and then subcloned into the SalI site of vector pCB7 (42). The vector pCB7 contains the cytomegalovirus promoter, a hygromycin B (GIBCO BRL, Gaithersburg, MD) resistance element, and an SV-40 polyadenylation site.

Cell Culture and Transfection

AtT-20 cells were cultured in DME supplemented with 10% FBS. Cells were transfected with Rab3D-pcB7 and Rab3D N135I-pcB7 using the Lipofectin Reagent (GIBCO BRL) according to the manufacturer's instructions. Stably transfected colonies were selected by growth in presence of hygromycin B (GIBCO BRL) used at a dilution of 1:1,000. Colonies were tested for expression of exogenous Rab3D and Rab3D N135I proteins by Western blot with Rab3D antibody. We selected four clonal cell lines for further studies: A3C1 and A3C4 cells, which express identical levels of Rab3D N135I; C6 cells, which express 20-fold more exogenous Rab3D than the endogenous protein; and C2 cells, which were transfected with *Rab3D*-pcB7 plasmid and hygromycin B resistant, but did not overexpress wild-type Rab3D.

Immunofluorescence Staining

For immunofluorescence analysis, AtT-20 cells were grown on poly-L-lysine–coated coverslips for at least 24 h, briefly washed with PBS at room temperature, and then fixed for 20 min at room temperature in PBS containing 4% parafomaldehyde. AtT-20 cells were then permeabilized with PBS solution containing 0.2% vol/vol Triton X-100 for 10 min at room temperature, and then washed three times with PBS. Incubations with primary and secondary antibodies were done as described before (26). We used affinity-purified rabbit polyclonal antibodies against Rab3D at 1:100 dilution and monoclonal antibodies against ACTH at 1:1,000 dilution. Cy3-conjugated donkey anti–mouse IgG and FITC-conjugated donkey anti–rabbit IgG were used at a final concentration of 30 μg/ml. Confocal microscopy was performed with a scanning laser confocal attachment (model LSM 410; Carl Zeiss, Inc., Thornwood, NY) mounted on an inverted fluorescence microscope (model 100 TV Axiovert; Carl Zeiss, Inc.). Optical sections were 1 μm thick. Images were processed using Adobe Photoshop software (Adobe Systems, Inc., San Jose, CA).

Electron Microscopy

Cells were grown on coverslips in the same conditions as for optical microscopy. After a brief rinse in PBS, cells attached to a glass surface were fixed with 2.5% glutaraldehyde in 0.1 M phosphate buffer, pH 7.3, for 10 min at room temperature, and then for 20 min at 4°C. Cells were then rinsed in 0.1 M phosphate buffer, pH 7.3, postfixed with 1% osmium tetroxide in the same buffer for 1 h at 4°C, dehydrated in ascending alcohols, and then treated with propylene oxide. After embedding in Araldite (Electron Microscopy Sciences, Ft. Washington, PA), ultrathin sections of the cell monolayers were cut with a Reichert OM ultramicrotome. Sections were stained with uranyl and lead citrate, and then examined with an electron microscope (model 100S or 1200EX; JEOL USA, Inc., Peabody, MA). To quantitate positioning of dense core granules, 10 electron micrographs of AtT-20 and A3C1 cells were taken at random. The magnification of the electron micrograph negatives was 5,000× and that of the final printed micrographs was 10,000×. Quantitation of the number of dense core granules per micron length of plasma membrane and the number of dense core granules per μm^2 perinuclear cytoplasm was done using the Mop-Videoplan Image analysis system (Kontron Electronic Group, Munich, Germany).

Immunoelectron Microscopy

Immunogold labeling of agarose-embedded AtT-20 cells was performed using the broken cells method described elsewhere (9, 21). To obtain broken AtT-20 cells, preconfluent AtT-20 cells cultured in one 72-cm^2 flask were washed in PBS, and then scraped in 2 ml of ice-cold homogenization buffer containing 250 mM sucrose, 25 mM KCl, 2 mM EGTA, and 10 mM sodium phosphate, pH 6.5. Cells were lightly homogenized by passing them through a 20-gauge needle with a 5-ml syringe twice. Cells were fixed by addition of 15 vol of ice-cold fixative solution containing 0.3 M sucrose, 3% paraformaldehyde, 0.25% glutaraldehyde, and 5 mM sodium phosphate, pH 6.5. Cells were kept in fixative solution for 30 min, pelleted by centrifugation at 1,000 *g* for 10 min, and then resuspended in 4 vol of 120 mM sodium phosphate, pH 7.5. The entire procedure was carried out at 4°C. Broken cells were agarose embedded as described (9). Incubations of agarose-embedded samples with affinity-purified Rab3D antibodies at a dilution of 1:20 was done as described (21). For gold immunolabeling, 10 nm colloidal gold-conjugated protein A was used at 1:20 dilution.

ACTH Release Assay

70% confluent cells plated at least 72 h before the assay were rinsed three times with DME medium at 37°C. Cells were then incubated for 1 h at 37°C with or without 5 mM 8-Br-cAMP in 0.4 ml buffer A, pH 7.4, containing 150 mM NaCl, 20 mM Hepes, 0.70 mM $CaCl_2$, 5 mM KCl, 1 mM $MgCl_2$, and 0.1 mg/ml bovine serum albumin. The cell medium was collected and then proteins were precipitated by the addition of 1.6 ml of acetone. After overnight incubation at −20°C, precipitates were collected by centrifugation in an Eppendorf centrifuge (Brinkman Instruments, Westbury, NY) operated at maximal speed for 20 min. Samples were resuspended in 0.16 ml and 20–80 μl were used for SDS-PAGE electrophoresis. After blotting onto nitrocellulose, bands were visualized with anti-ACTH monoclonal antibody by the enhanced chemiluminescence method as described elsewhere (37).

Results

Rab3A and Rab3D Immunofluorescence Distribution with Respect to the ACTH-containing Compartment

We investigated the relative distribution of Rab3D and ACTH by double immunofluorescence experiments analyzed by confocal microscopy. ACTH immunofluorescence was more concentrated at the perinuclear Golgi re-

1. *Abbreviations used in this paper*: SNAP-25, synaptomal-associated protein of 25 kD; VAMP, vesicle-associated membrane protein.

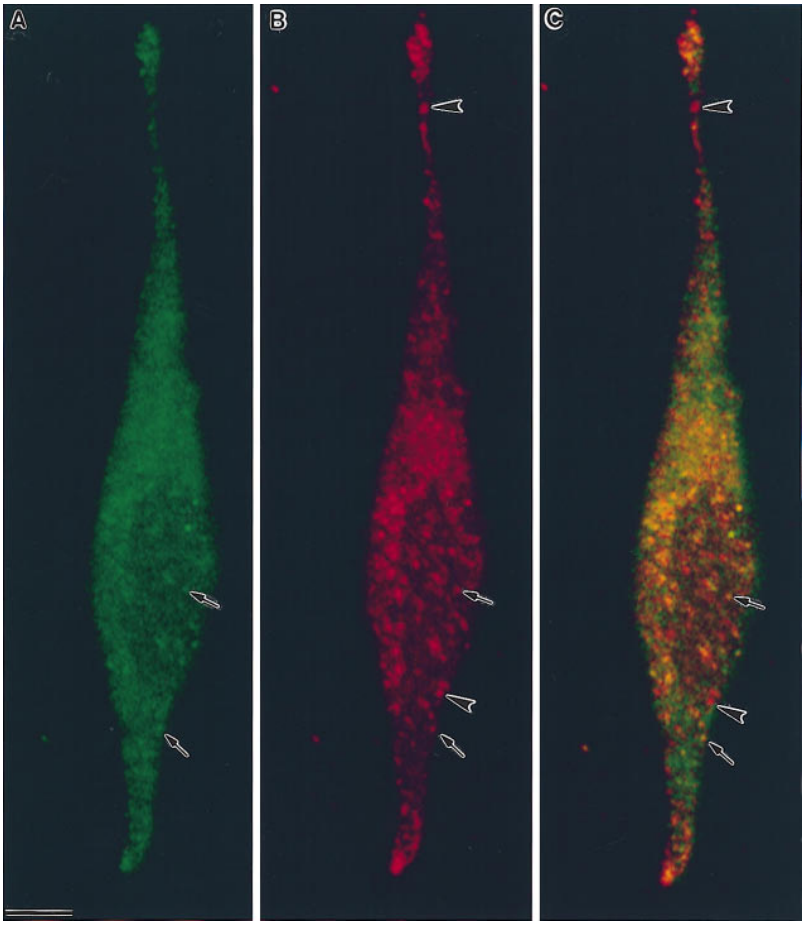

Figure 1. Distribution of Rab3D and ACTH in AtT-20 cells. Double immunofluorescence analysis of Rab3D (*A*, *green*) and ACTH (*B*, *red*) distribution by confocal microscopy. Overlay (*C*). Cells were labeled with affinity-purified rabbit antipeptide antibody against Rab3D (1:100 dilution) and mouse monoclonal antibodies against ACTH (1:1,000) dilution. The second costaining was performed with FITC-conjugated donkey anti–rabbit IgG and Cy3-conjugated donkey anti–mouse IgG. Puncta where Rab3D and ACTH staining coincide are indicated by arrows; puncta of predominant ACTH immunoreactivity are indicated by arrowheads. Bar, 5 μM.

gion and at the tips of the neurite-like processes (Fig. 1 *B*, *red*). In the same cell, Rab3D staining (*A*), is a more uniform green fluorescence in the cytoplasm of the cell body, the processes, and the tips. When the two images were merged (*C*), we found: (*a*) yellow puncta of Rab3D and ACTH fluorescence more concentrated at the cell body (*arrows*) and at their tips, indicating colocalization of Rab3D and ACTH; (*b*) puncta of red ACTH fluorescence that do not correspond to puncta of green fluorescence (*arrowheads*), and (*c*) areas of prevalent green Rab3D immunoreactivity, particularly evident in the cytoplasm of the processes. The immunofluorescence pattern was similar in C6 cells overexpressing exogenous Rab3D (data not shown).

To determine whether Rab3D is associated with dense core granules, we did immunoelectronmicroscopy on agarose-embedded, broken AtT-20 and C6 cells expressing wild-type Rab3D. We could not detect any gold staining in samples from untransfected AtT-20 cells. In samples from C6 cells expressing exogenous wild-type Rab3D, immunogold particles were found associated with dense core granules (Fig. 2). Plasma membranes near the granules were unlabeled (*arrowheads*, *A* and *C*). Nuclear membranes (data not shown), mitochondria (*m*), and viruses (*v*) were also unlabeled. From the immunofluorescence and the immunoelectronmicroscopy data, we conclude that a fraction of Rab3D is associated with dense core granules.

Expression of Rab3D N135I in AtT-20 Cells

To analyze the function of Rab3D in AtT-20 cells, we generated a mutated isoform of Rab3D, Rab3D N135I. In Fig. 3, it is shown that in the homogenate of A3C1 cells transfected with Rab3D N135I, there are two Rab3D-immunoreactive bands. The upper band comigrates with endogenous Rab3D in untransfected AtT-20 cells. The lower band corresponds to Rab3D N135I. Thus, Rab3D N135I, like Rab3A N135I and Rab3B N135I, has a higher electrophoretic mobility than the wild-type protein (4, 50). By measuring the recovery of Rab3D in the pellet and the supernatant fractions of the experiment shown in Fig. 3, we estimated that >90% of cellular wild-type and mutated Rab3D is associated with membranes. We find that Rab3D N135I, like Rab3D (26), cannot be solubilized from membranes by incubation in carbonate buffer at pH 11.5. Thus, membrane-bound Rab3D N135I is an integral membrane component, like Rab3D. Two Rab3D-immunoreactive bands are detectable in the supernatant fraction from A3C1 cells. The lower band has the same mobility as Rab3D N135I in the pellet fraction of A3C1 cells, and presumably corresponds to cytosolic, isoprenylated Rab3D N135I. The upper Rab3D-immunoreactive band in the A3C1 supernatant may correspond to soluble endogenous Rab3D and/or to unprenylated Rab3D N135I. This possibility is based on the observation that unprenylated

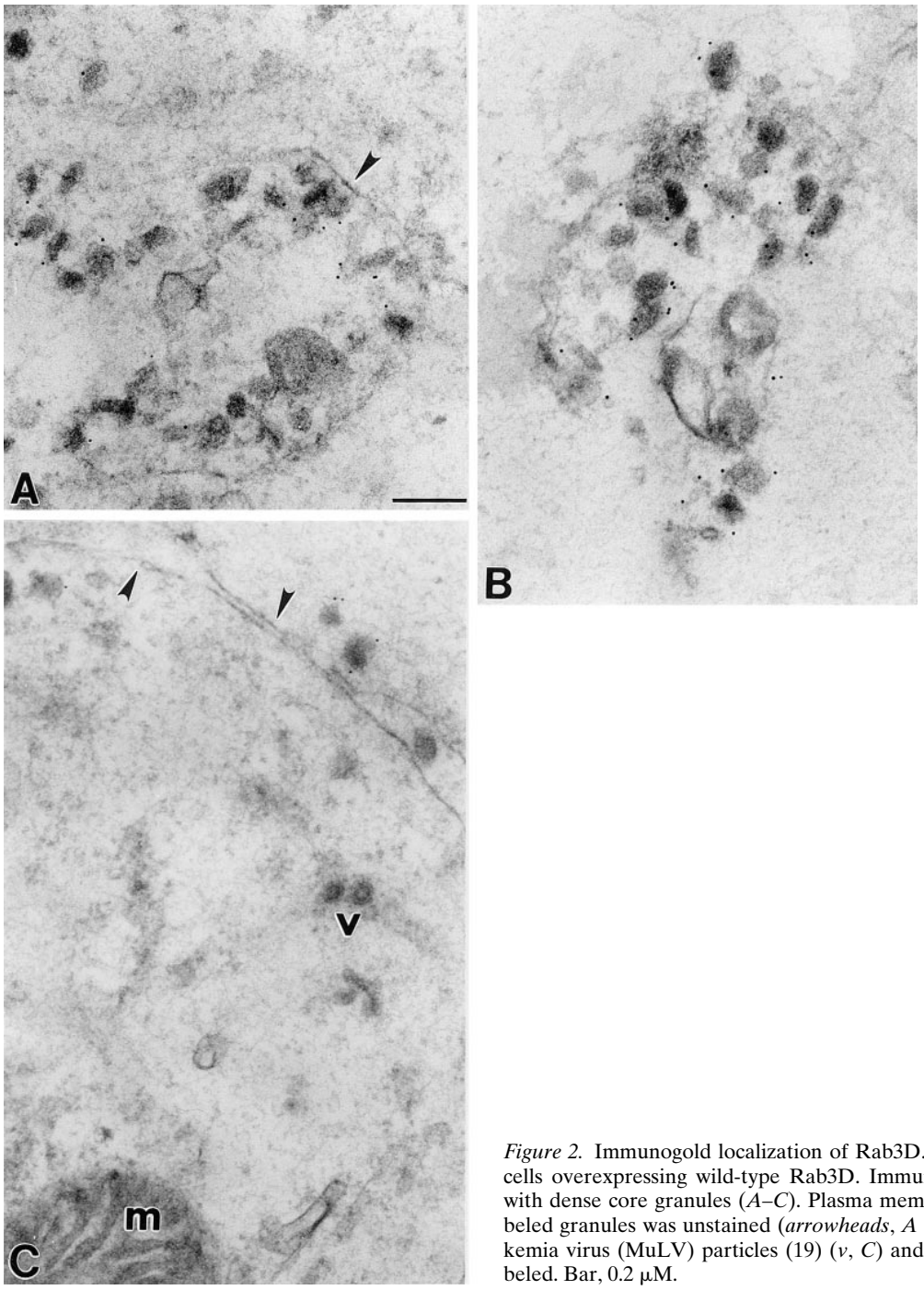

Figure 2. Immunogold localization of Rab3D. Immunogold staining of broken cells overexpressing wild-type Rab3D. Immunogold particles were associated with dense core granules (*A–C*). Plasma membrane found in the vicinity of labeled granules was unstained (*arrowheads*, *A* and *C*). Endogenous murine leukemia virus (MuLV) particles (19) (*v*, *C*) and mitochondria (*m*, *C*) were unlabeled. Bar, 0.2 μM.

GTPases migrate slower than the prenylated proteins after SDS-PAGE electrophoresis (23).

Distribution of Dense Core Granules in Cells Expressing Rab3D N135I

Mutations in the GTPase domain of individual Rab proteins affect vesicular traffic at distinct sites of the secretory pathway. Since Rab3D is found associated with dense core granules, we asked if there were differences in the distribution and/or morphology of these organelles in AtT-20 cells versus A3C1 cells expressing the presumed dominant-negative isoform Rab3D N135I. In the electron micrographs of Fig. 4, the distribution of dense core granules for each cell type is illustrated. For AtT-20 cells (Fig. 4, *arrows*, *C* and *D*), dense core granules are clearly positioned near the plasma membrane of the cell body (*arrowheads*). Dense core granules of similar size are accumulated at the tips of the processes (data not shown). In A3C1 cells expressing Rab3D N135I, the majority of dense core granules are scattered in the cytoplasm (Fig. 4, *A* and *B*). We could observe accumulation of dense core granules at the tips of the processes of A3C1 cells (data not shown). We quantified the relative distibution of granules found near the plasma membrane and in the perinuclear cytoplasm of AtT-20 cells and A3C1 cells (Fig. 5). The data indicate

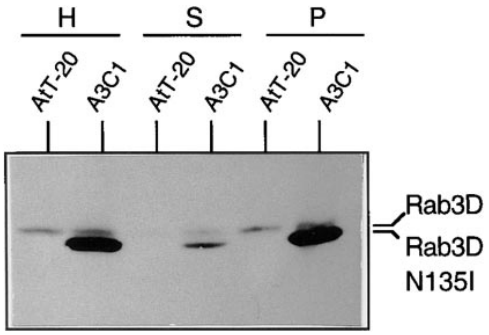

Figure 3. Rab3D N135I is predominantly membrane bound. One 10-cm diam plate of AtT-20 or A3C1 cells transfected with Rab3D N135I was rinsed twice with ice-cold homogenization buffer containing 250 mM sucrose, 10 mM Hepes buffer, pH 7.4, 2 mM EGTA, and 1 mM EDTA. Cells were scraped in 0.8 ml homogenization buffer containing 300 μg/ml PMSF, 1.5 μg/ml leupeptin, and 6 μg/ml aprotinin, homogenized with 12 strokes in a Teflon pestle homogenizer (0.08–0.13-mm clearance), and then centrifuged at 95,000 rpm in a TLA 100.2 rotor of the Beckman TL Optima centrifuge (Beckman Instruments, Fullerton, CA). The pellet was resuspended in 0.8 ml of homogenization buffer. The lanes of the SDS-PAGE gel were loaded with 40 μg protein of AtT-20 and A3C1 cells homogenates (*H*, 1% of total homogenate fraction), pellets (*P*, 2% of total membrane fraction) and supernatants (*S*, 4% of total supernatant fraction). The blot was probed with antibodies against Rab3D (1:1,000 dilution). Bands were visualized by enhanced chemiluminescence.

that expression of mutated Rab3D N135I in AtT-20 cells inhibits recruiting dense core granules at the cell surface. Immunofluorescence experiments with antitubulin antibodies show a similar pattern in A3C1 and AtT-20 cells (data not shown). Thus, impaired positioning of granules near the plasma membrane in A3C1 cells is not because of obvious changes in the arrangement of the cytoskeleton.

Regulated and Constitutive Secretion of ACTH in A3C1 Cells

The release of precursor and mature ACTH by AtT-20 and A3C1 cells is illustrated in Fig. 6. The proteins secreted into the medium were analyzed by Western blot analysis. AtT-20 cells and A3C1 cells expressing mutated Rab3D secrete similar amounts of 32-kD ACTH precursors and 23-kD intermediate forms (35), and there is little or no increase in the intensity of these bands after stimulation with 5 mM 8-Br-cAMP (*top*). Incubation with 5 mM 8-Br-cAMP induces a sharp increase in secretion of the mature, glycosylated 13-kD form of ACTH (11) in the medium of AtT-20 cells (*bottom*). Stimulation of A3C1 cells with 8-Br-cAMP induced only a modest increase of mature ACTH secretion, indicating that expression of Rab3D N135I inhibits regulated hormone secretion. In our hands, the 5-kD unglycosylated form of ACTH was less abundant than the 13-kD glycosylated form of ACTH in the culture medium of stimulated AtT-20 cells (data not shown). However, the 5-kD ACTH band is more abundant than the 13-kD band in AtT-20 cell extracts, as shown below. It is possible that proteolytic enzymes secreted in the cell medium cleave the unglycosylated form of ACTH during the 1-h incubation at 37°C.

Fig. 7 is a summary of the ACTH secretion data obtained from several experiments. In mock transfected cells (clone C2) or cells expressing 20-fold excess of exogenous wild-type Rab3D (clone C6), regulated secretion of ACTH is as efficient as in untransfected AtT-20 cells. Inhibition of 8-Br-cAMP-induced ACTH secretion occurs only in clones A3C1 and A3C4, which express similar levels of Rab3D N135I. These experiments show that expression of Rab3D N135I, but not overexpression of wild-type Rab3D (clone 6), is able to inhibit mature ACTH secretion.

Cells expressing Rab3D N135I may be unable to secrete mature ACTH because they produce less of the mature hormone than wild-type AtT-20 cells. To test this possibility, we analyzed the content of ACTH immunoreactive species in AtT-20 and A3C1 cell extracts. P2 fractions, which contain dense core granules (18) from both cell lines, were analyzed by Western blot with the ACTH antibody (Fig. 8, *left*). AtT-20 and A3C1 cells have identical amounts of 29-, 34-, and 23-kD ACTH precursor and intermediate forms (36). These cells also have the same levels of mature glycosylated and unglycosylated ACTH (the 13- and 5-kD protein bands, respectively). Thus, expression of mutated Rab3D has no effect on the ability of AtT-20 cells to express proopiomelanocortin and to process precursor ACTH to the mature hormone. These data indicate that expression of Rab3D N135 inhibits vesicular traffic in the ACTH secretory pathway, but does not interfere with the process of precursor maturation.

The inability of cells expressing Rab3D N135I to secrete mature ACTH may be because of a lack of differentiation. Fractions P2 from AtT-20 cells and A3C1 cells were analyzed in the same experiment for their content of synaptotagmin, VAMP-2/synaptobrevin-2, SNAP-25, and Rab3A (Fig. 8, *right*). These proteins are thought to function in neurotransmission and other regulated secretory pathways (3, 40). The amount of synaptotagmin, VAMP-2/synaptobrevin-2, and SNAP-25 per milligram of protein is similar in A3C1 and AtT-20 cells. Our results indicate that A3C1 and AtT-20 cells differentiate to a similar extent. Rab3A levels in fraction P2 from A3C1 cells were fivefold lower than in fraction P2 from AtT-20 cells. This result is further analyzed in Fig. 10.

Cells expressing Rab3D N135I may be unable to secrete ACTH because the hormone is not packaged in dense core granules. P2 fraction contains partially purified dense core granules (18). We further fractionated P2 membranes from AtT-20 and A3C1 cells by sucrose density gradient centrifugation. The distribution of ACTH precursor and ACTH hormone was identical in samples from AtT-20 cells and A3C1 cells. ACTH precursor (34-kD form) migrated as a wide peak in fractions 6–11. Processed ACTH hormones (13- and 6-kD forms) were concentrated in fractions 9 and 10 (Fig. 9). Thus, ACTH hormone is packaged in organelles of similar density in AtT-20 cells and A3C1 cells. Synaptotagmin is a membrane component of synaptic vesicles and neuropeptide-containing dense core vesicles (47). After sucrose density centrifugation of P2 fractions, synaptotagmin immunoreactivity distributed as a unique peak comigrating with ACTH hormone. This observation indicates that the pool of synaptotagmin recovered in fraction P2 is associated with dense core granules. Thus, the amount of ACTH hormone per unit membrane

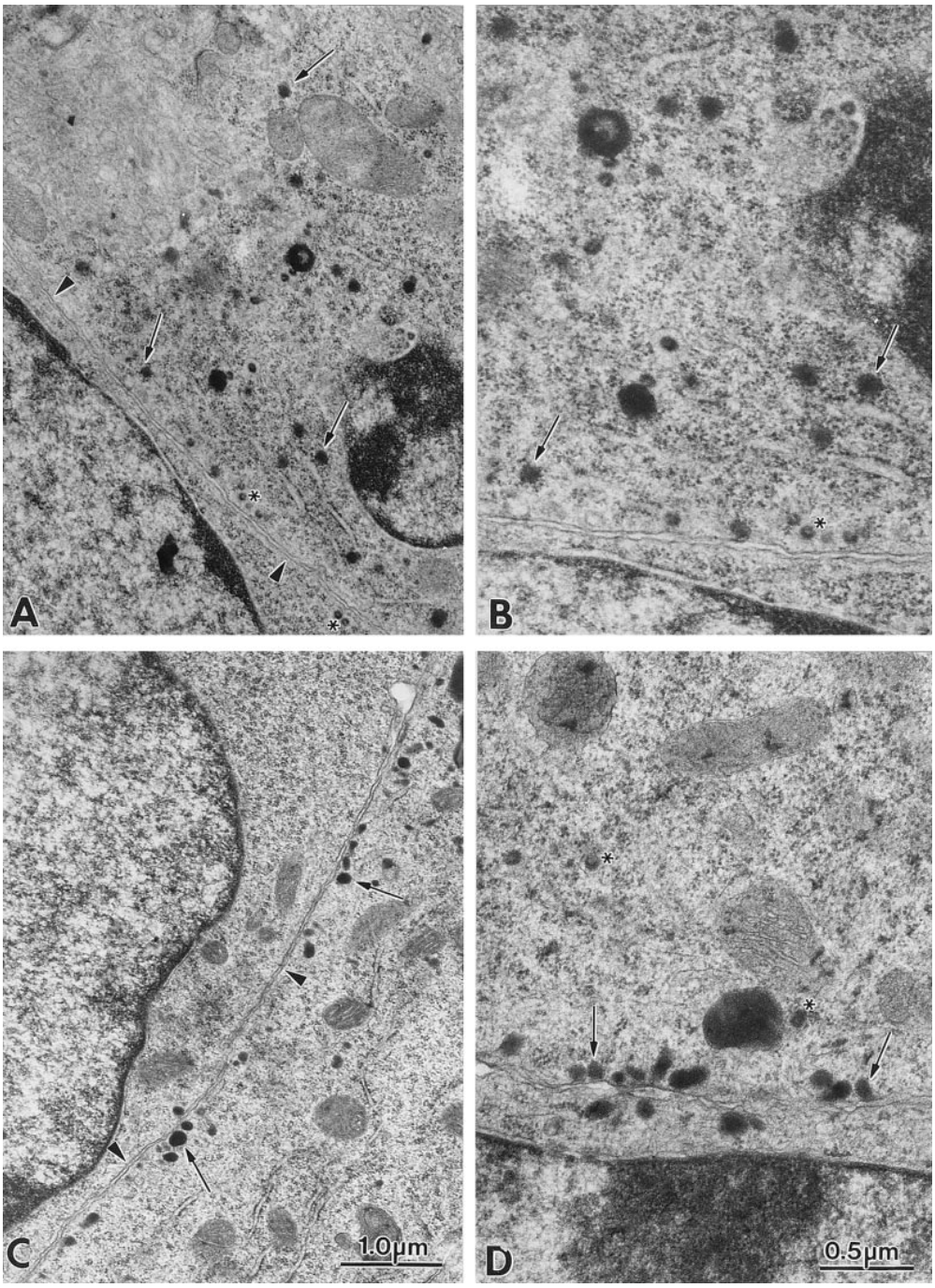

Figure 4. Distribution of dense core granules in AtT-20 cells and in cells expressing Rab3D N135I. Electron micrograph of the cell body of A3C1 cells (*A* and *B*) and AtT-20 cells (*C* and *D*). In AtT-20 cells the majority of dense core granules (*arrows*) at the cell body are positioned near the plasma membrane (*arrowheads*). In A3C1 cells granules are dispersed in the cytoplasm. The small-diameter, clear vesicles approaching the plasma membrane (*asterisk*) in A3C1 and AtT-20 cells correspond to the endogenous murine leukemia virus (MuLV) particles (19). The virus particles could also be visualized in clusters in the extracellular space. *A* and *C* (or *B* and *D*) are at the same magnification.

component of granules (refer to Fig. 8) seems to be similar or identical in AtT-20 and A3C1 cells. We conclude that in A3C1 cells expressing Rab3D N135I, packaging of processed ACTH hormone in dense core granules occurs with the same efficiency as in control cells.

Rab3A levels are 10-fold lower in the P2 fraction from A3C1 cells as compared to the same fraction from AtT-20 cells. In Fig. 10 *A*, it is shown that total amounts of Rab3A in the homogenate from A3C1 cells is only twofold less abundant than in the control. After 30 min of centrifugation at 400,000 *g*, we find that the supernatants (*S*) of A3C1 and AtT-20 cells contain similar levels of Rab3A immunoreactivity. However, there is approximately five-fold less Rab3A protein in the membrane-containing pellet (*P*) from A3C1 than in the same fraction from AtT-20 cells. In the same experiment, we find that there is no inhibition of Rab4 binding to the pellet fraction of A3C1 cells. These data indicate that in A3C1 cells, there is a relative inability of Rab3A to bind to cellular organelles, rather than a defect in the biosynthesis of Rab3A. The lower levels of Rab3A in the homogenate of A3C1 cells may be because of enhanced degradation of mislocalized Rab3A. In Fig. 10 *B*, it is shown that P2 fraction from C6 cells, which expresses high levels of wild-type Rab3D, has normal levels of Rab3A protein. Thus, inhibition of Rab3A association with membranes is because of the N135I mutation,

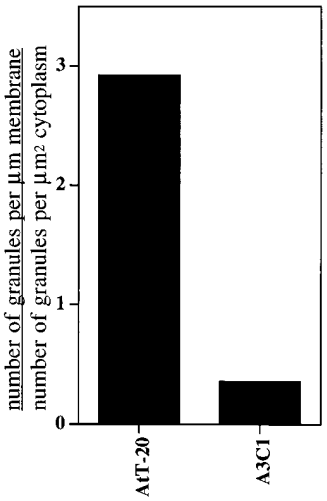

Figure 5. Comparison of granules distribution along the plasma membrane in A3C1 cells and AtT-20 cells. The relative concentration of granules along the plasma membrane was calculated as the ratio of granules/μm of plasma membrane to granules/μm^2 of cytoplasm. The granules along the plasma membrane (granules/μm membrane) are those found within 200 nm of the cell surface. In AtT-20 cells, 186 granules were counted along 696.1 μm of plasma membrane (0.267 granules/μm). In the same cells, 121 granules were found in 1,326.2 μm^2 of cytoplasm (0.091 granules/μm^2). In A3C1 cells, 84 granules were counted along 736.4 μm of plasma membrane (0.114 granules/μm). In the same cells, 379 granules were found in 1,184.0 μm^2 of cytoplasm space (0.320 granules/μm^2).

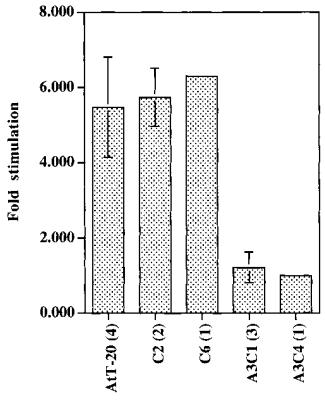

Figure 7. Quantitation of ACTH secretion by AtT-20 cells and AtT-20 cells expressing Rab3D N135I. The cell lines used for the experiments were: untransfected AtT-20 cells; cells transfected with *Rab3D*-pcB7 plasmid which did not overexpress wild-type Rab3D (clone *C2*); AtT-20 cells overexpressing wild-type Rab3D (clone *C6*); AtT-20 cells expressing Rab 3D N135I (clones *A3C1* and *A3C4*). The intensity of the 13-kD ACTH band was measured as described in *Materials and Methods.* Error bars represent SEM. The number of experiments is indicated in parenthesis.

rather than to overexpression of Rab3D. Expression of mutated Rab3D N135I does not inhibit association of endogenous wild-type Rab3D to P2 membranes. These data indicate that mutated Rab3D N135I specifically inhibits association of Rab3A with an intracellular membrane compartment.

Discussion

Our immunofluorescence experiments indicate that a fraction of endogenous Rab3D colocalizes with ACTH immunoreactivity in AtT-20 cells. These data are in agreement with the findings of Chavez et al. (6) in that exogenous, epitope tagged Rab3D colocalizes with ACTH at the tips of AtT-20 cells and at the cell body. By immunoelectron microscopy in AtT-20 cells expressing exogenous Rab3D, we find that the protein is specifically associated with dense core granules. These data indicate that Rab3D functions at late stages in the ACTH secretory pathway.

To test whether Rab3D is involved in the ACTH secretory pathway, we transfected AtT-20 cells with a presumed dominant-negative mutant of Rab3D, Rab3D N135I. We then asked whether there were differences in the morphology and/or distribution of dense core granules in cells expressing mutated Rab3D as compared to control cells. In untransfected AtT-20 cells, most of the granules in the cell body are found near the plasma membrane. This observation is consistent with other reports indicating that in neuroendocrine PC12 cells, the majority of dense core granules are docked at the plasma membrane (36). In A3C1 cells expressing Rab3D N135I, dense core granules were randomly localized in the cytoplasm of the cell body. The defect in granule positioning is not because of obvious changes in the architecture of the cytoskeleton, since the

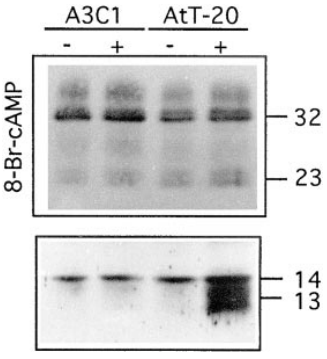

Figure 6. Regulated ACTH secretion is inhibited in AtT-20 cells expressing Rab3D N135I. The lanes of SDS-PAGE gel (15% acrylamide) were loaded with polypeptides secreted by AtT-20 cells during a 1-h incubation with or without 8-br-cAMP. The blot was probed with monoclonal antibody against ACTH 1:1,000. Bands were visualized by enhanced chemiluminescence. The upper and lower halves of the blot were exposed for autoradiography for 10 s and 1 min, respectively. The specificity of bands detected with a monoclonal antibody against ACTH was controlled in preliminary experiments by using the antibody in presence of 1 μM 1–24 ACTH peptide. Detection of all protein bands with the exception of a 14-kD band (Fig. 8, *bottom*) was abolished by incubation with the ACTH peptide.

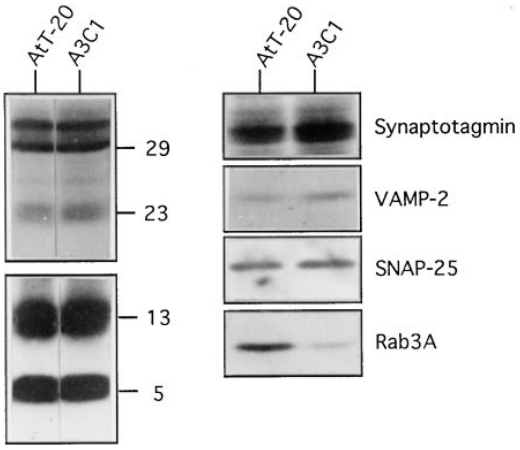

Figure 8. AtT-20 and A3C1 cells have similar amounts of ACTH precursor and mature forms. 50 μg of P2 fractions from AtT 20 and A3C1 cells were loaded into SDS-PAGE gel. Blots on the left panel were probed with ACTH monoclonal antibodies. The upper and the lower halves of the blot were exposed for autoradiography as described in Fig. 6. Blots on the right panel were probed with synaptotagmin at 1:1,000 dilution, VAMP-2 antibodies at 1:5,000 dilution, SNAP-25 antibodies at 1:200 dilution, and Rab3A antibodies at 1:1,000 dilution.

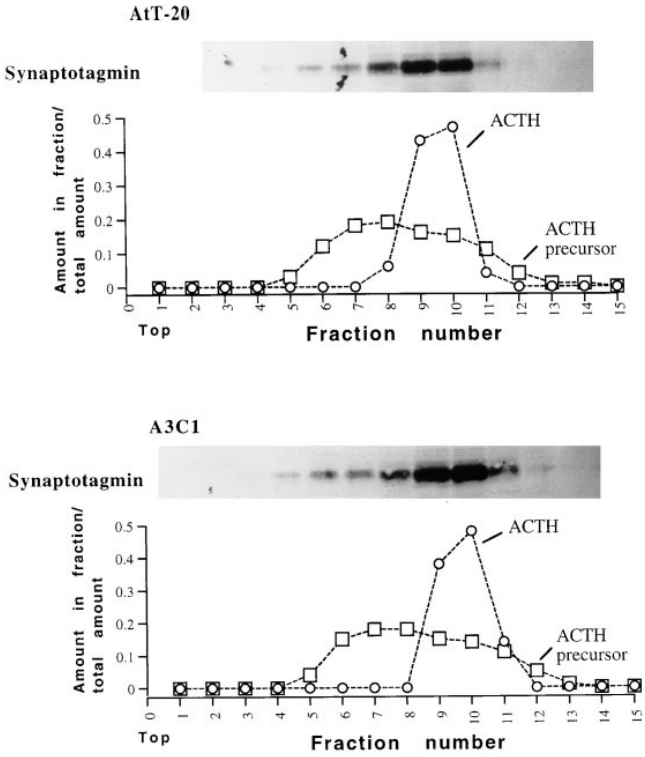

Figure 9. Equilibrium sucrose density analysis of P2 fractions from AtT-20 and A3C1 cells. P2 fraction obtained from four 10 cm-diam plates of AtT-20 or A3C1 cells were resuspended in 0.45 ml homogenization buffer (see Fig. 11) and loaded onto an 11-ml continuous 10–60 wt/vol sucrose gradient. After centrifugation for 17 h in a Beckman SW-41 rotor at 4°C fractions (0.8 ml) were taken from the top. Acetone was added to 0.2-ml aliquots of each fraction, proteins were precipitated for 16 h at −20°C, resuspended in sample buffer, and then loaded into a 15% acrylamide SDS-PAGE gel. Blots of gels containing AtT-20 and A3C1 samples were probed with synaptotagmin and ACTH antibodies. The distribution of 13-kD ACTH hormone (*graph*, *open circles*) and 34-kD ACTH precursor (*graph*, *open squares*) was determined by densitometry of the autoradiograms.

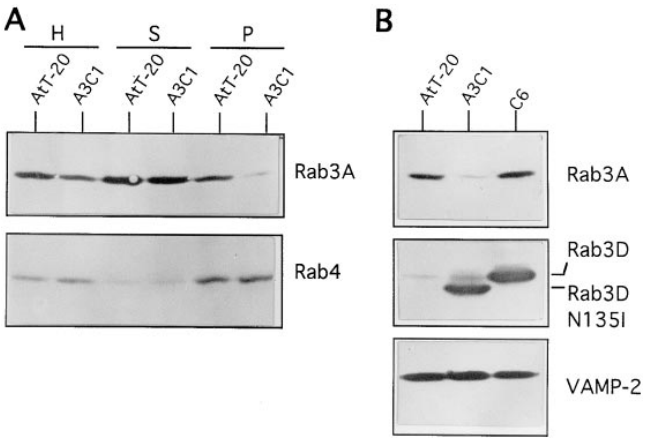

Figure 10. Distribution of Rab3A in subcellular fractions from AtT-20 and A3C1 cells. Homogenates, pellets, and supernatant fractions of AtT-20 and A3C1 cells were obtained as in Fig. 3. The lanes of the SDS-PAGE gel (*A*) were loaded with 40 μg protein of AtT-20 and A3C1 cell homogenates (*H*), pellets (*P*), and supernatants (*S*). The blot was probed with the monoclonal antibodies against Rab3A Cl 42.2 (1:1,000 dilution) and rabbit polyclonal antibody against Rab4 (1:1,000 dilution). 40 μg of P2 fractions from AtT-20 cells, A3C1 cells expressing Rab3D N135I, and C6 cells expressing exogenous Rab3D were loaded into SDS-PAGE gels. Blots were probed with Rab3A, Rab3D, and VAMP-2 antibodies at 1:1,000 dilution. Bands were visualized by enhanced chemiluminescence.

distribution of tubulin immunoreactivity (data not shown) is identical in cells expressing endogenous and mutated Rab3D.

In cells expressing Rab3D N135I, regulated secretion of ACTH hormone is blocked. However, untransfected AtT-20 and A3C1 cells expressing mutated Rab3D release identical levels of hormone precursors. These results indicate that Rab3D N135I inhibits regulated, but not constitutive, secretion. AtT-20 and A3C1 cells expressing Rab3D N135I process the same fraction of ACTH precursors into mature ACTH hormone. In both cell lines, the hormone is packaged in organelles with the same density. We conclude that expression of mutated Rab3D does not inhibit localization of ACTH to dense core granules. In A3C1 cells kept in basal conditions, we do not find higher levels of mature ACTH hormone than in AtT-20 cells. This result indicates that spontaneous release of processed ACTH hormone from granules occurs at a similar rate in unstimulated AtT-20 and A3C1 cells.

In A3C1 cells expressing Rab3D N135I, there are low levels of Rab3A associated with membranes. We have shown that the inability of Rab3A to bind to membranes is not a result of Rab3D overexpression, but a direct consequence of the mutation. Expression of Rab3D N135I does not impair association of Rab4 with membranes or even the binding of endogenous, wild-type Rab3D to P2 membranes. We conclude that expression of mutated Rab3D specifically impairs the ability of Rab3A to associate with cellular organelles. Rab3A binds to membranes of dense core granules in adrenal medullary cells and insulin-secreting cells (7, 8, 34). It is reasonable to hypothesize that expression of mutated Rab3D may impair association of Rab3A to ACTH-containing granules. This may be at least one of the defects that make dense core granules of AtT-20 cells expressing mutated Rab3D unable to exocytose. More work is necessary to understand whether Rab3A binds to synaptic-like microvesicles and/or to dense core granules in AtT-20 cells, and how expression of Rab3D N135I affects Rab3A association with these organelles.

Expression of Rab3D N135I in AtT-20 cells seems to induce the formation of "defective granules" that are separated from the Golgi, have normal density and ACTH content, but are unable to position near the plasma membrane or to exocytose. We speculate that these defective granules may lack components necessary for efficient vesicle docking and exocytosis. Another possibility is that in cells expressing mutated Rab3D, granules cannot release membrane components that function as clamps to prevent exocytosis.

We thank R. Jahn for the gift of antibodies against VAMP-2 and Rab3A, P. van der Sluijs for the gift of antibodies against Rab4, T. Swayne, A. Nistri, and L. Khiroug for the images obtained with the confocal microscope, T.E. McGraw for many helpful dicussions during the peparation of this work, and Dr. A.-J. Silverman for reading the manuscript.

This work has been funded in part by a grant from the American Diabetes Association and by a Grant-In-Aid from the American Heart Association, New York City Affiliate.

Received for publication 19 November 1996 and in revised form 18 November 1997.

References

1. Baldini, G., T. Hohl, H.Y. Lin, and H.F. Lodish. 1992. Cloning of a Rab3 isotype predominantly expressed in adipocytes. *Proc. Natl. Acad. Sci. USA.* 89:5049–5052.
2. Baldini, G., P.E. Scherer, and H.F. Lodish. 1994. Nonneuronal expression of Rab3A: induction during adipogenesis and association with different intracellular membranes than Rab3D. *Proc. Natl. Acad. Sci. USA.* 92: 4284–4288.
3. Bennett, M.K., and R.H. Scheller. 1994. A molecular description of synaptic vesicle membrane trafficking. *Annu. Rev. Biochem.* 63:63–100.
4. Brondyk, W.H., C.J. McKiernan, E.S. Burstein, and I.G. Macara. 1993. Mutants of Rab3A analogous to oncogenic Ras mutants. *J. Biol. Chem.* 268:9410–9415.
5. Castillo, P.E., R. Janz, T.C. Sudhof, T. Tzounopoulos, R.C. Malenka, and R.A. Nicoll. 1997. Rab3A is essential for mossy fiber long-term potentiation in the hippocampus. *Nature.* 388:590–593.
6. Chavez, R.A., S.G. Miller, and H.H. Moore. 1996. A biosynthetic secretory pathway in constitutive secretory cells. *J. Cell Biol.* 133:1177–1191.
7. Darchen, F., A. Zahraoui, F. Hammel, M.P. Monteils, A. Tavitian, and D. Scherman. 1990. Association of the GTP-binding protein Rab3A with bovine adrenal chromaffin granules. *Proc. Natl. Acad. Sci. USA.* 87:5692–5696.
8. Darchen, F., J. Senyshyn, W.H. Brondyk, D.J. Taatjes, R.W. Holz, J.P. Henry, J.P. Denizot, and I.G. Macara. 1995. The GTPase Rab3a is associated with large dense core vesicles in bovine chromaffin cells and rat PC12 cells. *J. Cell Sci.* 108:1639–1649.
9. De Camilli, P., S.M. Harris, Jr., W.B. Huttner, and P. Greengard. 1983. Synapsin I (Protein I), a nerve terminal-specific phosphoprotein. II. Its specific association with synaptic vesicles demonstrated by immunocytochemistry in agarose-embedded synaptosomes. *J. Cell Biol.* 96:1355–1373.
10. Edelmann, L., P.I. Hanson, E.R. Chapman, and R. Jahn. 1995. Synaptobrevin binding to synaptophysin: a potential mechanism for controlling the exocytotic fusion machine. *EMBO (Eur. Mol. Biol. Organ.) J.* 14:224–231.
11. Eipper, B.A., and R.E. Mains. 1977. Peptide analysis of a glycoprotein form of adrenocorticotropic hormone. *J. Biol. Chem.* 252:8821–8832.
12. Fischer von Mollard, G., G.A. Mignery, M. Baumert, M.S. Perin, T.J. Hanson, P.M. Burger, R. Jahn, and T.C. Sudhof. 1990. Rab3 is a small GTP-binding protein exclusively localized to synaptic vesicles. *Proc. Natl. Acad. Sci. USA.* 87:1988–1992.
13. Fischer von Mollard, G., B. Stahl, A. Khokhlatchev, T.C. Sudhof, and R. Jahn. 1994. Rab3C is a synaptic vesicle protein that dissociates from synaptic vesicles after stimulation of exocytosis. *J. Biol. Chem.* 269:10971–10974.
14. Fischer von Mollard, G., B. Stahl, C. Li, T.C. Sudhof, and R. Jahn. 1994. Rab proteins in regulated exocytosis. *Trends Biochem. Sci.* 19:164–168.
15. Fischer von Mollard, G., T.C. Sudhof, and R. Jahn. 1991. A small GTP-binding protein dissociates from synaptic vesicles during exocytosis. *Nature.* 349:79–81.
16. Geppert, M., V.Y. Bolshakov, S.A. Siegelbaum, K. Takei, P. De Camilli, R.E. Hammer, and T.C. Sudhof. 1994. The role of Rab3A in neurotransmitter release. *Nature.* 369:493–497.
17. Geppert, M., Y. Goda, C.F. Stevens, and T.C. Sudhof. 1997. The small GTP-binding protein Rab3A regulates a late step in synaptic vesicle fusion. *Nature.* 387:810–814.
18. Gumbiner, B., and R.B. Kelly. 1981. Secretory granules of an anterior pituitary cell line, AtT-20, contain only mature forms of corticotropin and beta-lipotropin. *Proc. Natl. Acad. Sci. USA.* 78:318–322.
19. Gumbiner, B., and R.B. Kelly. 1982. Two distinct intracellular pathways transport secretory and membrane glycoproteins to the surface of pituitary tumor cells. *Cell.* 28:51–59.
20. Holz, R.W., W.H. Brondyk, R.A. Senter, L. Kuizon, and I.G. Macara. 1994. Evidence for the involvement of Rab3A in $Ca(2^+)$-dependent exocytosis from adrenal chromaffin cells. *J. Biol. Chem.* 269:10229–10234.
21. Jena, P.J., F.D. Gumkowsky, E.M. Konieczko, G. Fischer von Mollard, R. Jahn, and J.D. Jamieson. 1994. Redistribution of a Rab3-like GTP-binding protein from secretory granules to the Golgi complex in pancreatic acinar cells during regulated exocytosis. *J. Cell Biol.* 124:43–53.
22. Johannes, L., P.M. Lledo, M. Roa, J.D. Vincent, J.P. Henry, and F. Darchen. 1994. The GTPase Rab3a negatively controls calcium-dependent exocytosis in neuroendocrine cells. *EMBO (Eur. Mol. Biol. Organ.) J.* 13:2029–2037.
23. Kato, K., A.D. Cox, M.M. Hisaka, S.M. Graham, J.E. Buss, and C.J. Der. 1992. Isoprenoid addition to Ras protein is the critical modification for its membrane association and transforming activity. *Proc. Natl. Acad. Sci. USA.* 89:6403–6407.
24. Lledo, P.M., P. Vernier, J.D. Vincent, W.T. Mason, and R. Zorec. 1993. Inhibition of Rab3B expression attenuates $Ca(2^+)$-dependent exocytosis in rat anterior pituitary cells. *Nature.* 364:540–544.
25. Mains, R.E., and B.A. Eipper. 1978. Coordinate synthesis of corticotropins and endorphins by mouse pituitary tumor cells. *J. Biol. Chem.* 253:651–655.
26. Martelli, A.M., R. Bareggi, G. Baldini, P.E. Scherer, H.F. Lodish, and G. Baldini. 1995. Diffuse vesicular distribution of Rab3D in the polarized neuroendocrine cell line AtT-20. *FEBS (Fed. Eur. Biochem. Soc.) Lett.* 368:271–275.
27. Matsui, Y., A. Kikuchi, J. Kondo, T. Hishida, Y. Teranishi, and Y. Takai. 1988. Nucleotide and deduced amino acid sequences of a GTP-binding protein family with molecular weights of 25,000 from bovine brain. *J. Biol. Chem.* 263:11071–11074.
28. Matsuuchi, L., K.M. Buckley, A.W. Lowe, and R.B. Kelly. 1988. Targeting of secretory vesicles to cytoplasmic domains in AtT-20 and PC-12 cells. *J. Cell Biol.* 106:239–251.
29. Matteoli, M., K. Takei, R. Cameron, P. Hurlbut, P.A. Johnston, T.C. Sudhof, R. Jahn, and P. De Camilli. 1991. Association of Rab3A with synaptic vesicles at late stages of the secretory pathway. *J. Cell Biol.* 115:625–633.
30. Ngsee, J.K., A.M. Fleming, and R.H. Scheller. 1993. A rab protein regulates the localization of secretory granules in AtT-20 cells. *Mol. Biol. Cell.* 4:747–756.
31. Oberhauser, A.F., J.R. Monck, W.E. Balch, and J.M. Fernandez. 1992. Exocytotic fusion is activated by Rab3a peptides. *Nature.* 360:270–273.
32. Padfield, P.J., W.E. Balch, and J.D. Jamieson. 1992. A synthetic peptide of the rab3a effector domain stimulates amylase release from permeabilized pancreatic acini. *Proc. Natl. Acad. Sci. USA.* 89:1656–1660.
33. Pfeffer, S.R. 1994. Rab GTPases: master regulators of membrane trafficking. *Curr. Opin. Cell Biol.* 6:522–526.
34. Regazzi, R., M. Ravazzola, M. Iezzi, J. Lang, A. Zahraoui, E. Andereggen, P. Morel, Y. Takai, and C.B. Wollheim. 1996. Expression, localization and functional role of small GTPases of the Rab3 family in insulin-secreting cells. *J. Cell Sci.* 109:2265–2273.
35. Roberts, J.L., M. Phillips, P.A. Rosa, and E. Herbert. 1978. Steps involved in the processing of common precursor forms of adrenocorticotropin and endorphin in cultures of mouse pituitary cells. *Biochemistry.* 17:3609–3618.
36. Schafer, T., U.O. Karli, F.E. Schweizer, and M.M. Burger. 1987. Docking of chromaffin granules—a necessary step in exocytosis? *Biosci. Rep.* 7:269–279.
37. Scherer, P.E., M.P. Lisanti, G. Baldini, M. Sargiacomo, C.C. Mastick, and H.F. Lodish. 1994. Induction of caveolin during adipogenesis and association of GLUT4 with caveolin-rich vesicles. *J. Cell Biol.* 127:1233–1243.
38. Simons, K., and M. Zerial. 1993. Rab proteins and the road maps for intracellular transport. *Neuron.* 11:789–799.
39. Stahl, B., G.F. von Mollard, C. Walch-Solimena, and R. Jahn. 1994. GTP cleavage by the small GTP-binding protein Rab3A is associated with exocytosis of synaptic vesicles induced by alpha-latrotoxin. *EMBO (Eur. Mol. Biol. Organ.) J.* 15:1799–1809.
40. Sudhof, T.C., P. De Camilli, H. Niemann, and R. Jahn. 1993. Membrane fusion machinery: insights from synaptic proteins. *Cell.* 75:1–4.
41. Tang, L.H., F.D. Gumkowski, D. Sengupta, I.M. Modlin, and J.D. Jamieson. 1996. Rab3D protein is a specific marker for zymogen granules in gastric chief cells of rats and rabbits. *Gastroenterology.* 110:809–820.
42. Thomas, D.C., C.B. Brewer, and M.G. Roth. 1993. Vesicular stomatitis virus glycoprotein contains a dominant cytoplasmic basolateral sorting signal critically dependent upon a tyrosine. *J. Biol. Chem.* 268:3313–3320.
43. Touchot, N., P. Chardin, and A. Tavitian. 1987. Four additional members of the ras gene superfamily isolated by an oligonucleotide strategy: molecular cloning of YPT-related cDNAs from a rat brain library. *Proc. Natl. Acad. Sci. USA.* 84:8210–8214.
44. Valentijin, J.A., D. Sengupta, F.D. Gumkowski, L.H. Tang, E.M. Konieczko, and J.D. Jamieson. 1996. Rab3D localizes to secretory granules in rat pancreatic acinar cells. *Eur. J. Cell Biol.* 70:33–41.
45. van der Sluijs, P., M. Hull, P. Webster, P. Male, B. Goud, and I. Mellman. 1992. The small GTP-binding protein rab4 controls an early sorting event on the endocytic pathway. *Cell.* 70:729–740.
46. Walch-Solimena, C., J. Blasi, L. Edelmann, E.R. Chapman, G.F. von Mollard, and R. Jahn. 1995. The t-SNAREs syntaxin 1 and SNAP-25 are present on organelles that participate in synaptic vesicle recycling. *J. Cell Biol.* 128:637–645.
47. Walch-Solimena, C., K. Takei, K.L. Marek, K. Midyett, T.C. Sudhof, P. De Camilli, and R. Jahn. 1993. Synaptotagmin: a membrane constituent of neuropeptide-containing large dense-core vesicles. *J. Neurosci.* 13:3895–3903.
48. Walworth, N., B. Goud, A. Kabcenell, and P. Novick. 1989. Mutational analysis of SEC 4 suggests a cyclical mechanism for the regulation of vesicular traffic. *EMBO (Eur. Mol. Biol. Organ.) J.* 8:1685–1693.
49. Weber, E., G. Berta, A. Tousson, P. St. John, M.V. Green, U. Gopalokrishnan, T. Jilling, E.J. Sorscher, T.S. Elton, D.R. Abramson, and K.L. Kirk. 1994. Expression and polarized targeting of a Rab3 isoform in epithelial cells. *J. Cell Biol.* 125:583–594.
50. Weber, E., T. Jilling, and K.L. Kirk. 1996. Distinct functional properties of Rab3A and Rab3B in PC12 neuroendocrine cells. *J. Biol. Chem.* 271: 6963–6971.
51. Zahraoui, A., N. Touchot, P. Chardin, and A. Tavitian. 1989. The human Rab genes encode a family of GTP-binding proteins related to yeast YPT1 and SEC4 products involved in secretion. *J. Biol. Chem.* 264: 12394–12401.